Volume 12 | Number 39 | 21 October 2016 | Pages 8061–8258

Soft Matter

www.softmatter.org

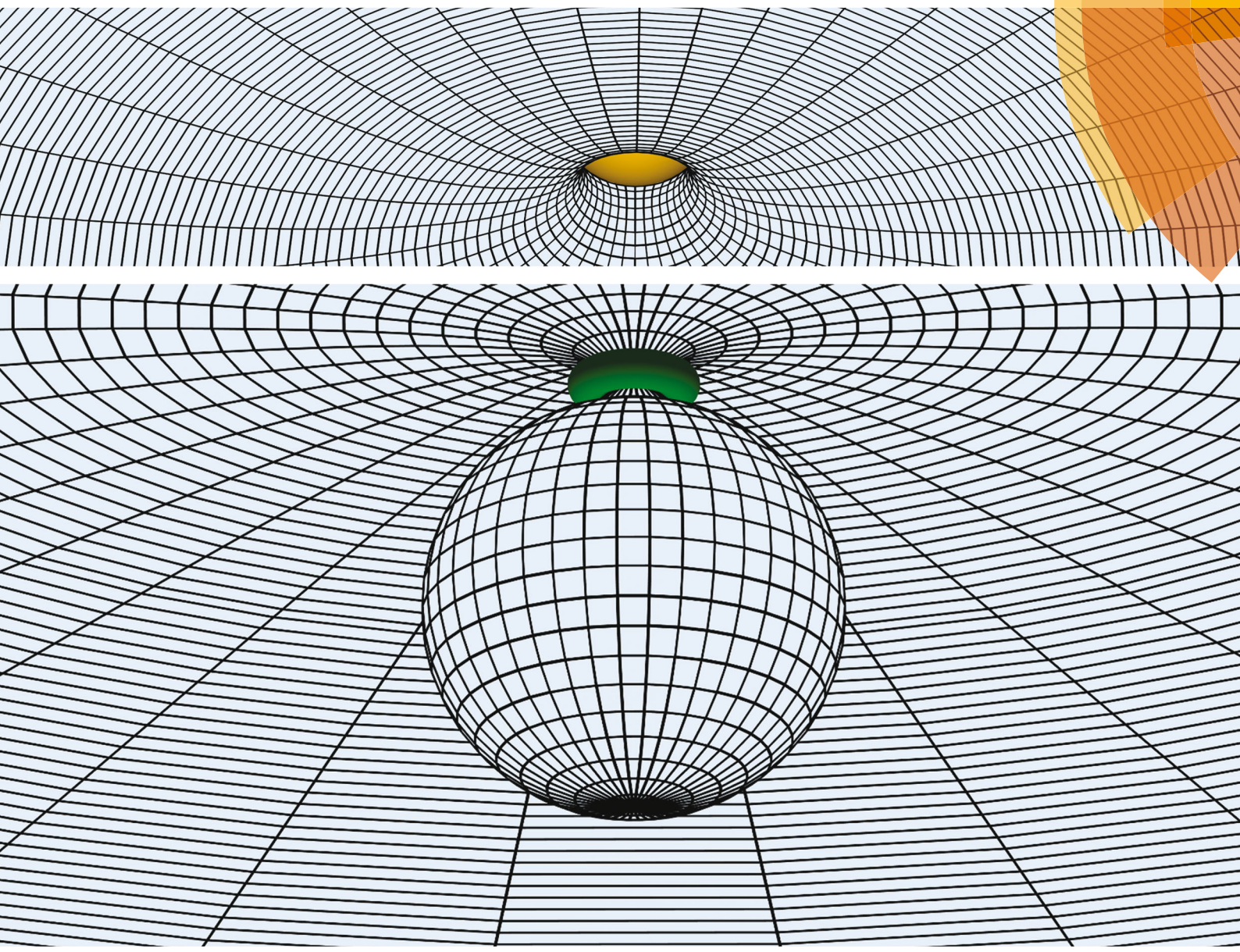

ISSN 1744-683X

ROYAL SOCIETY OF CHEMISTRY

PAPER
Jaime Agudo-Canalejo and Reinhard Lipowsky
Stabilization of membrane necks by adhesive particles, substrate surfaces, and constriction forces

175 YEARS

Soft Matter

PAPER

View Article Online
View Journal | View Issue

Cite this: *Soft Matter*, 2016, **12**, 8155

Stabilization of membrane necks by adhesive particles, substrate surfaces, and constriction forces

Jaime Agudo-Canalejo* and Reinhard Lipowsky*

Received 27th June 2016,
Accepted 2nd August 2016

DOI: 10.1039/c6sm01481j

www.rsc.org/softmatter

Membrane remodelling processes involving the formation and fission of small buds require the formation and closure of narrow membrane necks, both for biological membranes and for model membranes such as lipid bilayers. The conditions required for the stability of such necks are well understood in the context of budding of vesicles with bilayer asymmetry and/or intramembrane domains. In many cases, however, the necks form in the presence of an adhesive surface, such as a solid particle or substrate, or the cellular cortex itself. Examples of such processes in biological cells include endocytosis, exocytosis and phagocytosis of solid particles, the formation of extracellular and outer membrane vesicles by eukaryotic and prokaryotic cells, as well as the closure of the cleavage furrow in cytokinesis. Here, we study the interplay of curvature elasticity, membrane-substrate adhesion, and constriction forces to obtain generalized stability conditions for closed necks which we validate by numerical energy minimization. We then explore the consequences of these stability conditions in several experimentally accessible systems such as particle-filled membrane tubes, supported lipid bilayers, giant plasma membrane vesicles, bacterial outer membrane vesicles, and contractile rings around necks. At the end, we introduce an intrinsic engulfment force that directly describes the interplay between curvature elasticity and membrane-substrate adhesion.

1 Introduction

In the absence of external forces, liquid droplets attain spherical shapes that minimize their surface area and, thus, their interfacial free energy for a given droplet volume. In contrast to droplets, lipid vesicles formed by biomimetic or biological membranes can attain a large variety of different shapes that minimize the membranes' curvature energy for a given vesicle volume and membrane area. Particularly intriguing vesicle shapes are provided by two spheres connected by a narrow membrane neck that appears to be highly curved but does not contribute to the curvature energy of the vesicle membrane.[1–4] Such necks are formed by membranes with uniform composition,[1,5] by membranes with intramembrane domains,[6–8] and by membranes exposed to optical tweezers.[9] Furthermore, narrow membrane necks are also ubiquitous in biological cells. Indeed, such necks are observed prior to endo- and exocytosis,[10,11] phagocytosis,[12] cytokinesis,[13] as well as autophagosome formation.[14] In the latter processes, the neck formation is regulated by a complex network of proteins.[15,16]

The formation of membrane necks frequently occurs in the presence of adhesive particles or substrate surfaces, see Fig. 1.

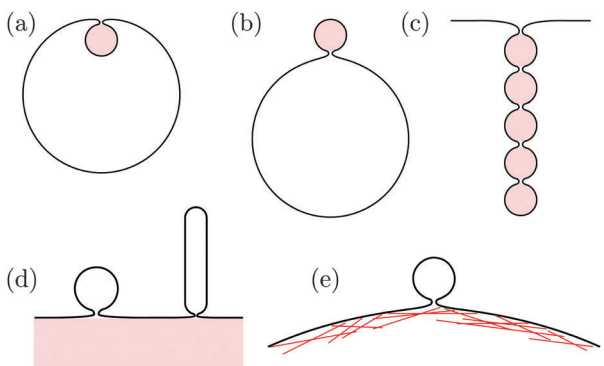

Fig. 1 Narrow membrane necks often form in the presence of adhesive particles or substrate surfaces: (a) endocytic and (b) exocytic engulfment of nanoparticles; (c) formation of necklace-like particle-filled tubes; (d) budding or tubulation of supported bilayers; and (e) formation of giant plasma membrane vesicles *via* chemically induced blebbing. In panels (a)–(c), the adhesive particles (pink) are located within the membrane buds and tubes. In panels (d) and (e), the membrane buds and tubes are not in direct contact with the adhesive substrates (pink) and the actin cortex.

On the one hand, membranes can engulf adhesive nanoparticles and then form particle-filled buds, the size of which is determined by the particle size, as displayed in Fig. 1(a and b).[17] These engulfment processes are essential for endocytosis and exocytosis

Theory & Biosystems, Max Planck Institute of Colloids and Interfaces, 14424 Potsdam, Germany. E-mail: jaime.agudo@mpikg.mpg.de, lipowsky@mpikg.mpg.de

by cellular membranes, can be used for drug delivery or medical imaging, and play an important role during viral infections. Analogous processes occur during phagocytosis of larger particles by specialized cells.

On the other hand, the plasma membrane of eukaryotic cells, which is in permanent contact with the adhesive actin cortex, can form extracellular vesicles such as exosomes, ectosomes, and apoptotic bodies, the size of which can vary over a wide range from 30 nm to a couple of micrometers.[18] During the formation of such a vesicle, the plasma membrane must detach from the actin cortex and bulge out towards the external medium until it forms a bud with a closed neck, which is eventually cleaved to release the vesicle. Particularly large cortex-free vesicles, so-called "giant plasma membrane vesicles", are formed *via* chemically induced blebbing, see Fig. 1(e).[19–22] A similar process is observed for Gram-negative bacteria during the secretion of "outer membrane vesicles". These bacteria have a cell wall that consists of a peptidoglycan layer sandwiched between two lipid bilayers. During the secretion process, a large segment of the outer bilayer detaches from the peptidoglycan layer, bulges out towards the external medium, and forms a spherical vesicle that is released from the prokaryotic cell.[23,24]

The processes of endocytosis and exocytosis can be mimicked in model systems, such as lipid or polymer vesicles in contact with adhesive particles, and the formation and closure of a narrow membrane neck has been observed to occur spontaneously in these systems, without the help of complex protein machinery as in biological cells.[25–29] Although not yet seen in experiments, particle-filled membrane tubes with narrow necks between the particles, see Fig. 1(c), have been predicted by numerical simulations.[30–32] Furthermore, formation and closure of membrane necks in the presence of adhesion also occurs during the unbinding of supported lipid bilayers *via* budding or tubulation, see Fig. 1(d).[33–37]

In the absence of adhesion, the mechanisms for the formation and closure of membrane necks during budding have been understood for quite some time, and typically require either a strong bilayer asymmetry leading to a spontaneous curvature of the membrane,[2,4] or phase separation in the membrane, giving rise to a line tension that contributes or even drives neck closure and budding.[7,39] In ref. 17 we showed, in the context of particle engulfment, that the presence of an adhesive surface helps in stabilizing closed necks and described a novel stability condition for such necks. In the present paper, we will rederive this stability condition using a particular parametrization of the neck shape, which will allow us to examine the energetics and geometry of narrow necks in a systematic manner, as well as to extend the applicability of the stability condition to other cases of interest.

The paper is organized as follows. The spontaneous curvature model with adhesion is introduced in Section 2.1. In Sections 2.2 and 2.3, we describe in detail the numerical process used to find the minimum energy shapes of a vesicle in contact with an adhesive particle, while in Section 2.4 we present the analytical model used in the analysis of shapes with narrow necks. The predictions of the analytical model are then validated in detail by numerical calculations in Sections 3.1 and 3.2, focusing on the case of particle engulfment. In the remaining sections, we extend the application of the analytical model to particle-filled membrane tubes, budding of supported lipid bilayers from homogeneous and patterned substrates, giant plasma membrane and outer membrane vesicle formation, and narrow necks in the presence of externally applied constriction forces.

Throughout the paper, endocytic and exocytic engulfment will be discussed in parallel. In all equations, the upper and lower signs of the $\pm$ or $\mp$ symbols will correspond to endocytic and exocytic engulfment, respectively.

2 Theoretical description and methods

2.1 Spontaneous curvature model with adhesion

The membrane is treated as a smooth, continuous surface and is studied within the framework of the well-established spontaneous curvature model.[2,40] Here, the membrane is described by two material parameters, namely its bending rigidity κ and its spontaneous curvature m. The bending energy of such a smooth membrane has the form

$$E_{\mathrm{be}} = 2\kappa \int \mathrm{d}A (M - m)^2 \tag{1}$$

where M is the mean curvature at each point of the membrane, and the integral represents an area integral over the whole membrane surface of the vesicle. The mean curvature is taken to be positive (negative) if the membrane bulges towards the exterior (interior) compartment of the vesicle. We will only consider transformations that leave the topology of the vesicle unchanged, which implies that the area integral over the Gaussian curvature provides a shape-independent constant.[40]

The adhesive interaction with the particle is included *via* a contact potential, with adhesive energy per unit area $W < 0$ and the adhesion energy[41]

$$E_{\mathrm{ad}} = -|W| A_{\mathrm{bo}} \tag{2}$$

where A_{bo} is the area of the membrane segment bound to the particle. The total energy to be considered is then given by

$$E = E_{\mathrm{be}} + E_{\mathrm{ad}}. \tag{3}$$

2.2 Numerical minimization of total energy

Our aim is to calculate the minimum energy shapes of a vesicle with fixed area A and enclosed volume V, attached to a rigid spherical particle of radius R_{pa}. The wrapping angle ϕ, as described in Fig. 2, represents the reaction coordinate of the engulfment process. In the context of particle engulfment, this wrapping angle can vary continuously between $\phi = 0$, corresponding to the non-adhering or free state of the particle, and $\phi = \pi$, corresponding to the particle being completely engulfed. In this completely engulfed state, the membrane bound to the particle is connected to the mother vesicle by a closed neck. In the continuum model considered here, the closed neck has zero thickness.

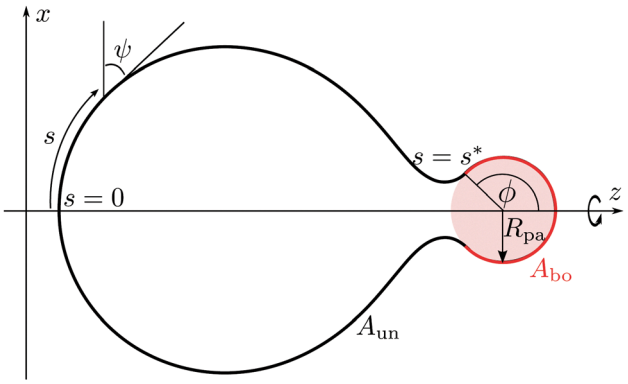

Fig. 2 Axisymmetric geometry and arc length parametrization of a vesicle in contact with a spherical particle (pink), used for the numerical minimization of the spontaneous curvature model with adhesion. The particle originates from the interior compartment corresponding to exocytic engulfment. The unbound part of the vesicle membrane (black), meets the bound part (red) smoothly at a certain wrapping angle ϕ. The bound part of the membrane has area A_{bo}, whereas the unbound part has area $A_{un} = A - A_{bo}$.

The bound segment of the vesicle membrane follows the contour of the particle, and thus assumes the shape of a spherical cap. This segment has the area

$$A_{bo} = 2\pi {R_{pa}}^2(1 - \cos\phi). \tag{4}$$

If we cut the spherical particle along the contact line, we obtain two spherical caps. The spherical cap adjacent to the bound membrane segment has the volume

$$V_{bo} = \frac{4\pi}{3}{R_{pa}}^3(2 + \cos\phi)\sin^4\frac{\phi}{2}. \tag{5}$$

Furthermore, the combined bending and adhesion energy of the bound membrane segment is given by

$$E_{bo} = [4\pi\kappa(1 \pm mR_{pa})^2 - 2\pi|W|{R_{pa}}^2](1 - \cos\phi). \tag{6}$$

The total energy E_{un} of the unbound part of the membrane is equal to its bending energy

$$E_{un} = 2\kappa\int \mathrm{d}A_{un}(M - m)^2. \tag{7}$$

In order to find the shape of the unbound segment that minimizes E_{un}, for a fixed value of ϕ, and satisfies the constraints on the total membrane area and enclosed volume of the vesicle, we must minimize the shape functional

$$F \equiv E_{un} + \Sigma(A - A_{bo}) - \Delta P(V \pm V_{bo}) \tag{8}$$

where Σ and ΔP are Lagrange multipliers for the area and volume constraints. The volume $V \pm V_{bo}$ is enclosed by the unbound membrane segment and the additional planar surface that spans the circular contact line.

Parametrizing the shape contour by its arc length s, see Fig. 2, the shape functional F becomes[2]

$$F = \int_0^{s^*} \mathrm{d}s\mathscr{L}\left(\psi, \dot\psi, x, \dot x, \gamma\right) \tag{9}$$

with the 'Lagrangian' function

$$\mathscr{L} \equiv \pi\kappa x\left(\dot\psi + \frac{\sin\psi}{x} - 2m\right)^2 + 2\pi\Sigma x + \pi\Delta P x^2\sin\psi + \gamma(\dot x - \cos\psi) \tag{10}$$

where $\gamma = \gamma(s)$ is a Lagrange multiplier function that serves to impose the geometrical constraint $\dot x = \cos\psi$, and the dot denotes a derivative with respect to the arc length s.

We now put the first variation δF in (9) equal to zero and obtain the Euler–Lagrange equations of (10), which are identical to the shape equations for a free vesicle[2] and have the form

$$\begin{aligned}
\dot\psi &= u \\
\dot u &= -\frac{u}{x}\cos\psi + \frac{\cos\psi\sin\psi}{x^2} + \frac{\gamma\sin\psi}{2\pi\kappa x} + \frac{\Delta P x\cos\psi}{2\kappa} \\
\dot\gamma &= \pi\kappa\left[(u - 2m)^2 - \frac{\sin^2\psi}{x^2}\right] + 2\pi\Sigma + 2\pi\Delta P x\sin\psi \\
\dot x &= \cos\psi
\end{aligned} \tag{11}$$

These equations are subject to the initial conditions

$$\psi(0) = 0, \quad u(0) = u_0, \quad \gamma(0) = 0, \quad x(0) = 0. \tag{12}$$

We can augment the system of equations in (11) with the equations for the area and volume as given by

$$\begin{aligned}
\dot A &= 2\pi x \\
\dot V &= \pi x^2\sin\psi
\end{aligned} \tag{13}$$

with initial conditions

$$V(0) = 0, \quad A(0) = 0. \tag{14}$$

We then have a system of six first-order differential equations with six initial conditions. There are, however, four unknown parameters: Σ, ΔP, u_0 and s^*. These are used to satisfy the four boundary conditions

$$\begin{aligned}
\psi(s^*) &= \pi \pm \phi \\
x(s^*) &= R_{pa}\sin\phi \\
A(s^*) &= A - A_{bo} \\
V(s^*) &= V \pm V_{bo}
\end{aligned} \tag{15}$$

at $s = s^*$, which enforce the constraints in area and volume, and a smooth matching between the unbound and bound segment of the vesicle membrane.

The problem is thus well-posed, and can be solved using a non-linear shooting procedure. The numerical integration of eqn (11) and (13), with initial conditions in eqn (12) and (14), is performed using a Runge–Kutta method, while the search for the values of Σ, ΔP, u_0 and s^* that satisfy the boundary conditions in (15) is carried out using Newton's method. The case of a vesicle that can freely adjust its volume is included by setting $\Delta P = 0$ in (11) and ignoring the boundary condition for the volume $V(s^*)$ in (15).

2.3 Parameters of the vesicle–particle system

The system depends on six parameters corresponding to three geometric parameters, namely the particle radius R_{pa}, the total membrane area A and enclosed volume V of the vesicle as well as three material parameters, namely the bending rigidity κ, the spontaneous curvature m and the adhesive strength $|W|$. However, choosing the bending rigidity κ as the basic energy scale and the vesicle size

$$R_{ve} \equiv \sqrt{A/4\pi} \tag{16}$$

as the basic length scale, we can explore the whole parameter space *via* four dimensionless parameters as defined by

$$r_{pa} \equiv R_{pa}/R_{ve}, \quad v \equiv 3V/(4\pi {R_{ve}}^3), \quad \bar{m} \equiv mR_{ve} \tag{17}$$

and

$$w \equiv |W|{R_{pa}}^2/\kappa. \tag{18}$$

If the solution contains no osmotically active solutes, the volume of the vesicle can adjust freely, and the three reduced parameters r_{pa}, $\bar{m}$ and w completely define the system.

The computation then proceeds as follows: for fixed values of r_{pa}, $\bar{m}$ and v, the total energy of the system $E(\phi)$ as a function of ϕ is obtained from the bending energy $E_{un}(\phi)$ of the unbound membrane segment resulting from the shooting method, together with the bending and adhesive energies, $E_{bo}(\phi)$, of the particle-bound segment, given by (6), so that $E(\phi) \equiv E_{un}(\phi) + E_{bo}(\phi)$. Closed necks will be stable or unstable if $E(\phi)$ has a boundary minimum or maximum, respectively, at $\phi = \pi$.

2.4 Analysis of narrow membrane necks

The limiting case of a particle close to complete engulfment with wrapping angle $\phi \lesssim \pi$, in which the bound part of the membrane is connected to the mother vesicle by a narrow neck, can be understood in the context of a specific shape parametrization that has been previously used for the budding of uniform membranes[4] and of intramembrane domains.[7,39] The corresponding shape contour is displayed in Fig. 3, and is divided into four regions I–IV. Region I is a hemisphere of radius R_1 representing the least perturbed part of the vesicle. The neck is described by regions II and III, which correspond to unduloid segments. Region IV is a spherical cap of radius R_{pa} and aperture angle ϕ, representing the segment bound to the particle. Our model differs from the one in ref. 4 and 39 in that the aperture or wrapping angle ϕ can have any value in the range $\pi/2 \le \phi \le \pi$, instead of being fixed to $\phi = \pi/2$. This ϕ-range is essential in order to study necks in the presence of an adhesive particle.

Note that the piece-wise parametrization of the vesicle shape just described does not solve the shape equations as given by (11) and, thus, represents an approximation to the equilibrium shape of the vesicle. However, this parameterization leads to stability conditions for closed necks that are in excellent agreement with the lines of limit shapes as found numerically for the budding of uniform membranes[2–4] and of intramembrane domains.[7,39] This agreement implies that the parameterization correctly captures the asymptotic behavior of the system in the limit of small neck diameters. In general, the use of this piece-wise parametrization should always be scrutinized *a posteriori* by comparing its predictions with exact numerical results, see Section 3 below.

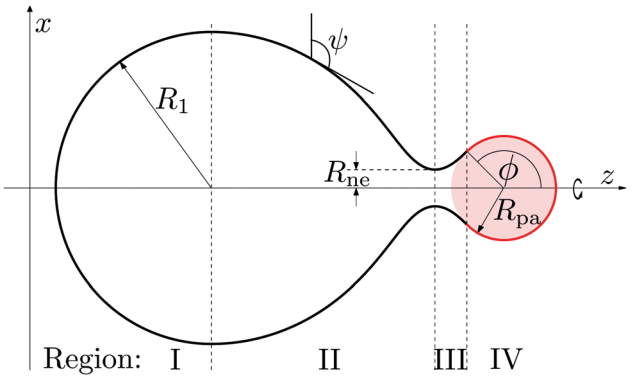

Fig. 3 Piece-wise parametrization for the shape contour of the vesicle membrane as used in the analytical study of narrow membrane necks for exocytic engulfment. All four membrane segments I, II, III, and IV have constant mean curvature. Segment I forms a hemisphere of radius R_1, segments II and III represent two unduloidal segments connected by a neck of radius R_{ne}, and segment IV is a spherical cap of radius R_{pa} and aperture angle ϕ. In the exocytic case depicted here, the spherical particle (pink) originates from the interior compartment.

The shape contour of the unduloidal segment II can be parametrized by

$$\sin\psi = \frac{1}{R_1 \mp R_{ne}}\left(x \mp \frac{R_1 R_{ne}}{x}\right) \quad \text{for } R_{ne} < x < R_1 \tag{19}$$

while the shape contour of the unduloidal segment III has the parametrization

$$\sin\psi = \frac{\mp 1}{R_2 + R_{ne}}\left(x + \frac{R_2 R_{ne}}{x}\right) \quad \text{for } R_{ne} < x < R_{pa}\sin\phi \tag{20}$$

where R_{ne} is the radius of the neck connecting the two spherical caps, R_1 is the radius of the spherical cap representing the unperturbed part of the vesicle and R_2 is given by

$$R_2 \equiv R_{pa}\frac{\sin^2\phi\left(1 - \dfrac{R_{ne}}{R_{pa}}\right)}{\sin^2\phi - \dfrac{R_{ne}}{R_{pa}}} \tag{21}$$

where R_{pa} is the radius of the particle.

The total area, enclosed volume and bending energy of such a trial contour can be readily calculated analytically for given values of R_1, R_{ne}, R_{pa} and ϕ. We are, however, primarily interested in the limit of narrow necks which corresponds to the inequality

$$\varepsilon \equiv R_{ne}/R_{pa} \ll 1. \tag{22}$$

Inspection of Fig. 3 shows that the neck radius R_{ne} tends to zero when the wrapping angle ϕ tends to π. More generally, when the shifted angle

$$\eta \equiv \pi - \phi \quad \text{with} \quad \sin\eta = \sin\phi \tag{23}$$

becomes small, the neck radius becomes small as well, with the condition $R_{ne} < R_{pa}\sin\eta$ or equivalently $\varepsilon < \sin\eta$ being always satisfied during the closure of the membrane neck. We will thus consider an expansion in powers of ε, taking into account that the dimensionless ratio $\sin^2\eta/\varepsilon$ is of order one. The total membrane area of the trial contour is found to be

$$A = 4\pi {R_1}^2\left(1 + \frac{{R_{pa}}^2}{{R_1}^2} \mp \frac{1}{2}\frac{R_{pa}}{R_1}\varepsilon + O\left(\varepsilon^2\log\varepsilon\right)\right). \quad (24)$$

Because we will consider variations of the contour for fixed total area A, the radius R_1 of the unperturbed part of the vesicle must obey the relation

$$R_1 = R_0\left(1 \pm \frac{1}{4}\frac{R_{pa}}{R_0}\varepsilon + O\left(\varepsilon^2\log\varepsilon\right)\right) \quad (25)$$

where R_0 is defined by $4\pi {R_0}^2 \equiv A - 4\pi {R_{pa}}^2$, corresponding to the radius of the unbound part of the vesicle in the limit of a fully closed neck with $\varepsilon = 0$. The total volume enclosed by the vesicle is

$$V = \frac{4\pi}{3}{R_0}^3\left(1 \mp \frac{{R_{pa}}^3}{{R_0}^3} + O\left(\varepsilon^2\log\varepsilon\right)\right). \quad (26)$$

The contour parametrization used here does not allow us to keep both the total area and the enclosed volume constant at the same time. For this reason, we consider a shape ensemble of variable volume at constant osmotic pressure difference ΔP. The total energy to be considered is then composed of a bending term, an adhesion term and a pressure term and given by

$$E = E_{be} + E_{ad} - \Delta PV. \quad (27)$$

In the exocytic case, the volume V includes the volume of the particle, even if the latter is not accessible to the aqueous solution enclosed by the vesicle. However, including the particle volume in V has no effect on the energy minimization, because it only adds the constant term $-\Delta P(4\pi/3){R_{pa}}^3$ to the total energy, and this term is independent of the vesicle shape.

An expansion of the total energy in terms of the parameter ε then leads to the expression

$$\begin{aligned}\frac{E(\varepsilon,\eta)}{8\pi\kappa} &= (1 - mR_0)^2 + \left(1 \pm mR_{pa}\right)^2 - \frac{|W|{R_{pa}}^2}{2\kappa} - \frac{\Delta P}{6\kappa}\left({R_0}^3 \mp {R_{pa}}^3\right)\\ &\quad - \frac{1}{2}\varepsilon\left(1 \pm 2mR_{pa} \mp \frac{R_{pa}}{R_0}\right) + \frac{1}{4}\frac{\varepsilon^2}{\sin^2\eta}\\ &\quad + \frac{1}{4}\frac{|W|{R_{pa}}^2}{2\kappa}\sin^2\eta + O\left(\varepsilon^2\log\varepsilon\right)\end{aligned} \quad (28)$$

which depends on the neck radius ε and the shifted wrapping angle η. In order to compare the analytical theory with the numerical calculations, we need to find the optimal shape of the vesicle, and thus the optimal neck size ε^*, that minimizes the energy for a given wrapping angle ϕ with small $\eta = \pi - \phi$. Because the quadratic term in ε in eqn (28) is always positive, for a given value of η, the energy will have a minimum at a finite positive value of ε only if the linear term in ε is negative, which implies the condition

$$1 \pm 2mR_{pa} \mp \frac{R_{pa}}{R_0} > 0. \quad (29)$$

Indeed, if this condition is not satisfied, membrane buds of radius R_{pa} or larger are stable even in the absence of the adhesive particle,[2,4] and our contour parametrization is no longer appropriate.

By imposing $\left.\frac{\partial E(\varepsilon,\eta)}{\partial\varepsilon}\right|_{\varepsilon=\varepsilon^*} = 0$, we obtain the optimal neck size

$$\varepsilon^* = \left(1 \pm 2mR_{pa} \mp \frac{R_{pa}}{R_0}\right)\sin^2\eta + O\left[\sin^4\eta\log\left(\sin^2\eta\right)\right] \quad (30)$$

which, as expected, is small whenever $\sin^2\eta$ is small, and has a meaningful value only if the inequality (29) is satisfied.

By substituting the value of ε^* into (28), we obtain the total energy $E(\eta) \equiv E(\varepsilon^*, \eta)$ as a function of the shifted wrapping angle η. The difference in energy between a configuration with a narrow open neck and one with a closed neck $\delta E(\eta) \equiv E(\eta) - E(0)$ is finally found to behave as†

$$\delta E(\eta) \approx 2\pi\kappa\sin^2\eta\left[\frac{|W|{R_{pa}}^2}{2\kappa} - \left(1 \pm 2mR_{pa} \mp \frac{R_{pa}}{R_0}\right)^2\right] \quad (31)$$

to first order in $\sin^2\eta$ with $\eta = \pi - \phi$ as in (23). The energy difference $\delta E(\eta)$ represents the excess energy (or reversible work) necessary to open up the closed neck.

It is interesting to note that the pressure term $-\Delta PV$ does not contribute to the expression in (31) because it is of higher order in $\sin^2\eta$. Alternatively, one could consider a shape ensemble in which the enclosed volume is kept constant, whereas the membrane area is variable at constant tension Σ, with a term ΣA added to the total energy. In the latter case, we similarly find that the tension only adds higher order terms in $\sin^2\eta$ to the energy, with eqn (30) and (31) remaining unaffected.

3 Neck stability for engulfed particles

3.1 Stability of closed necks for particle engulfment

We now proceed to compare the predictions of the analytical theory for narrow necks with numerical calculations. One of the most important consequences of eqn (31) is that completely engulfed particles with $\eta = \pi - \phi = 0$ and a closed neck are (meta)stable only if the energy $\delta E(\eta)$ increases with increasing η for small η, and unstable otherwise. Taking (31) together with the condition (29), we find that a closed neck adjacent to a completely engulfed particle is (meta)stable whenever

$$\sqrt{\frac{|W|{R_{pa}}^2}{2\kappa}} \geq 1 \pm 2mR_{pa} \mp \frac{R_{pa}}{R_0}. \quad (32)$$

One limitation of the contour parametrization used in our analytical treatment is that the shape of the mother vesicle must be spherical with radius R_0 in the limit of closed necks with ${R_{ne}}^* = 0$. This limiting geometry always applies to vesicles

† Here and below, the symbol $\approx$ stands for 'asymptotically equal'.

with a freely adjustable volume and $\Delta P = 0$ but not to vesicles with fixed enclosed volume. In the latter case, the mother vesicle may display non-spherical shapes such as prolate or oblate shapes after the engulfment of the particle. In order to consider this more general situation, we can replace $1/R_0$ in (32) by the local mean curvature, M', of the mother vesicle at the position of the neck. With a slight rearrangement of the different terms, we can rewrite the stability condition in the form

$$\sqrt{\frac{|W|}{2\kappa}} - \frac{1}{R_{\rm pa}} \pm M' \mp 2m \geq 0 \qquad (33)$$

where the upper and lower signs of the $\pm$ and $\mp$ symbols correspond again to endocytic and exocytic engulfment, respectively, see Fig. 1(a and b). The first term on the left hand side of (33) is equal to the inverse of the adhesion length R_W defined by

$$R_W \equiv \sqrt{2\kappa/|W|}. \qquad (34)$$

This length scale can vary from about 10 nm to a couple of microns as described in ref. 17. The equality in (33) represents the neck closure condition of a limit shape for which the open neck becomes closed.

The stability condition (33) was originally obtained in ref. 17, *via* a heuristic argument based on the continuity of the bending energy density across the neck, and was confirmed by extensive numerical calculations for vesicles with and without volume constraint. For planar membranes without spontaneous curvature, the condition (33) becomes simply $|W| \geq 2\kappa/{R_{\rm pa}}^2$, which describes the numerical results in ref. 42 for the engulfment of particles by planar membranes with a fixed membrane tension. If we consider a non-adhesive particle with $|W| = 0$, the neck closure condition given by the equality in (33) becomes $M' + M_{\rm bo} = 2m$ with the mean curvature $M_{\rm bo} \equiv \mp 1/R_{\rm pa}$ of the particle-bound membrane segment. The latter relation is identical with the ideal neck condition previously obtained[2,4] for the budding of homogeneous vesicles. Eqn (33) is therefore a generalization of this neck condition to membranes interacting with adhesive surfaces.

For the case of a pressureless vesicle with no volume constraint, the curvature of the (spherical) mother vesicle after complete engulfment is simply $M' = 1/\sqrt{{R_{\rm ve}}^2 - {R_{\rm pa}}^2}$, where $R_{\rm ve} = \sqrt{A/4\pi}$ is now equal to the radius of the (spherical) vesicle before engulfment of the particle. In Fig. 4, we plot the neck closure condition (33) as a function of particle size $r_{\rm pa}$ and adhesive strength w, for different values of the spontaneous curvature $\bar{m}$. Closed necks are stable and unstable for high and low values of the adhesive strength, respectively. The condition as given by eqn (33) has been quantitatively confirmed by numerical energy minimization for a large number of different parameter values. For endocytic engulfment, see Fig. 4(a), negative spontaneous curvatures favour the stability of closed necks, whereas positive spontaneous curvatures act to destabilize them. In contrast, for exocytic engulfment, closed necks are favoured by positive and suppressed by negative spontaneous curvatures, see Fig. 4(b).

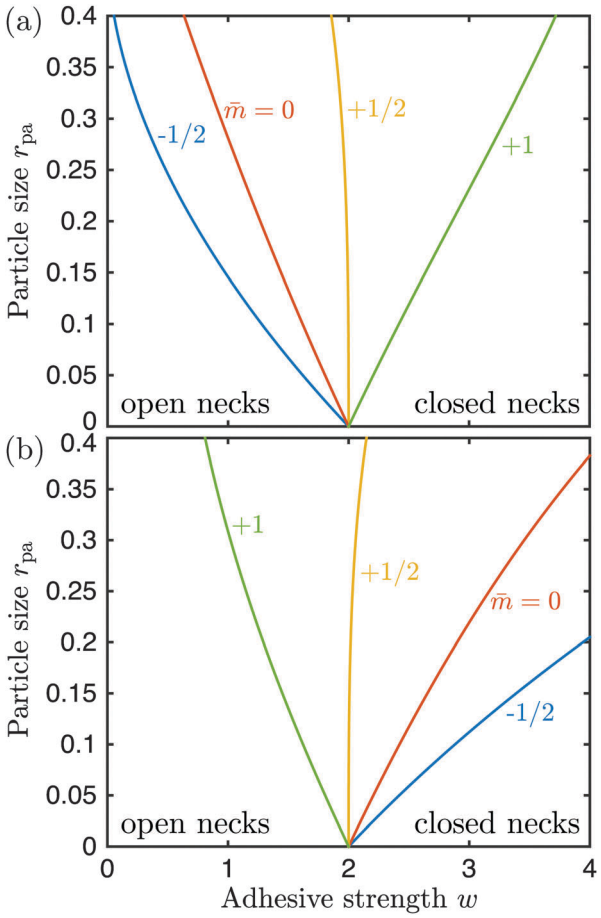

Fig. 4 Neck closure condition for (a) endocytic and (b) exocytic engulfment of a spherical particle, as a function of adhesive strength $w = |W|{R_{\rm ve}}^2/\kappa$ and particle size $r_{\rm pa} = R_{\rm pa}/R_{\rm ve}$. The different lines follow from (33) for different values of the spontaneous curvature $\bar{m} = mR_{\rm ve}$. The vesicle can freely adapt its volume corresponding to the osmotic pressure difference $\Delta P = 0$.

3.2 Energetics and geometry of neck opening

Using numerical computations, we now examine the expression (31) for the excess energy related to neck opening. In analogy to the derivation of eqn (33), we substitute $1/R_0$ in (31) by the local mean curvature M' of the (non-spherical) mother vesicle which leads to

$$\delta E(\eta) \approx 2\pi\kappa \sin^2\eta \left\{ \frac{|W|{R_{\rm pa}}^2}{2\kappa} - \left[1 \pm (2m - M')R_{\rm pa}\right]^2 \right\}. \qquad (35)$$

Eqn (35) implies that, to first order in $\sin^2\eta$, the excess energy for neck opening depends only on the local mean curvature M' of the membrane at the position of the neck, and is independent of the global shape of the vesicle.

We have validated eqn (35) by numerical energy minimization both for endocytic and exocytic engulfment, for vesicles with and without volume constraint, as well as for different spontaneous curvatures, particle sizes, and values of the adhesive strength. In all cases, eqn (35) provides the correct behaviour to first order in $\sin^2\eta$. A few examples are displayed in Fig. 5(a). For $\sin^2\eta = 0$, corresponding to complete engulfment with $\phi = \pi$, all numerical

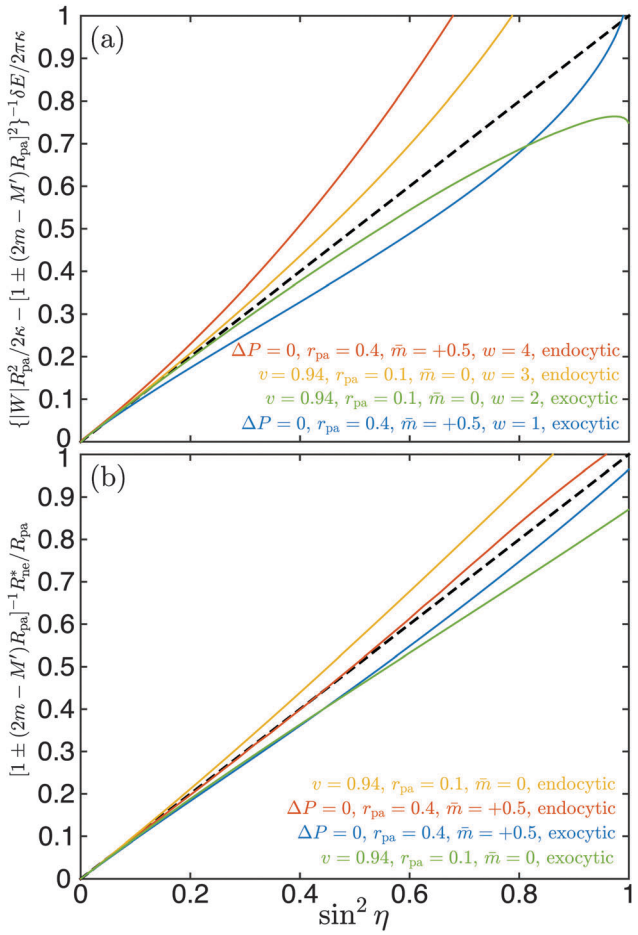

Fig. 5 (a) Excess energy δE for neck opening and (b) optimal neck radius R_{ne}^* as a function of $\sin^2\eta$ as obtained by numerical energy minimization. The shifted wrapping angle $\eta = \pi - \phi$ varies from $\eta = 0$ to $\eta = \pi/2$. The reduced volume $v = 0.94$ corresponds to prolate vesicles with fixed volume, the case $\Delta P = 0$ to spherical vesicles with adjustable volume. Both endocytic and exocytic engulfment are considered for two particle sizes $r_{pa} = 0.1$ and $r_{pa} = 0.4$ as well as for two spontaneous curvatures $\bar{m} = 0$ and $\bar{m} = 0.5$. In (a), a range of four different adhesive strengths w is examined. The scaling factors for the excess energy and the neck size, see lettering of the y-axes, correspond to eqn (35) and (36) respectively. As predicted by these equations, all lines have a common tangent at $\sin^2\eta = 0$, given by the black dashed line $y = x$.

lines have a common tangent as given by eqn (35). In all cases, the numerical results are reasonably well approximated by the analytical line in the range $0 \leq \sin^2\eta \leq 0.2$, corresponding to $\pi \geq \phi \geq 0.85\pi$.

Another testable prediction of the analytical theory is the behaviour of the optimal neck size R_{ne}^* as a function of wrapping angle ϕ. Following (30), again replacing $1/R_0$ by M' in order to generalize the result, and taking into account that $\varepsilon^* \equiv R_{ne}^*/R_{pa}$ we obtain

$$R_{ne}^* \approx \left[1 \pm (2m - M')R_{pa}\right] R_{pa} \sin^2\eta. \qquad (36)$$

For small $\eta = \pi - \phi$, the optimal radius of the neck depends only on the spontaneous curvature of the membrane, the particle size and the curvature of the mother vesicle at the position of the neck, irrespective of the global shape of the vesicle. We have also validated eqn (36) by numerical energy minimization. Some examples are shown in Fig. 5(b). As expected, all numerical lines have a common tangent at $\sin^2\eta = 0$. In all cases tested, the numerical results are reasonably well approximated by eqn (36) in the range $0 \leq \sin^2\eta \leq 0.4$, corresponding to $\pi \geq \phi \geq 0.78\pi$.

3.3 Stability of particle-filled membrane tubes

It is not difficult to extend the analytical treatment described in Section 2.4, and in particular the stability condition for closed necks (33), to membrane necks that form between two adhesive particles when two or more such particles are collectively engulfed by a larger vesicle into a tube-like structure, see Fig. 1(c). In such a situation, endocytic engulfment leads to membrane in-tubes, whereas exocytic engulfment leads to membrane out-tubes. First, consider a neck that belongs to a membrane out-tube with positive mean curvature of the particle-bound membrane segments. If a particle of radius R_{pa1} and adhesive strength $|W_1|$ is located on one side of the neck, and one of radius R_{pa2} and adhesive strength $|W_2|$ on the other side, a closed neck between the two particles will be stable if

$$\sqrt{\frac{|W_1|}{2\kappa}} + \sqrt{\frac{|W_2|}{2\kappa}} - \frac{1}{R_{pa1}} - \frac{1}{R_{pa2}} + 2m \geq 0. \qquad (37)$$

This relation implies that larger adhesive strengths, larger particles, and positive spontaneous curvatures favor the formation of closed necks for particle-filled out-tubes. Likewise, for a closed neck that belongs to a membrane in-tube with negative mean curvature of the particle-bound membrane segments, the stability relation for this neck is given by

$$\sqrt{\frac{|W_1|}{2\kappa}} + \sqrt{\frac{|W_2|}{2\kappa}} - \frac{1}{R_{pa1}} - \frac{1}{R_{pa2}} - 2m \geq 0. \qquad (38)$$

This relation implies that larger adhesive strengths, larger particles, and negative spontaneous curvatures favor closed necks for particle-filled in-tubes. If both particles are identical with radius $R_{pa1} = R_{pa2} = R_{pa}$ and adhesive strength $|W_1| = |W_2| = |W|$, the stability conditions simplify and become

$$\sqrt{\frac{|W|}{2\kappa}} - \frac{1}{R_{pa}} + m \geq 0 \quad \text{for out-tubes} \qquad (39)$$

and

$$\sqrt{\frac{|W|}{2\kappa}} - \frac{1}{R_{pa}} - m \geq 0 \quad \text{for in-tubes.} \qquad (40)$$

Particle-filled in- and out-tubes were first observed in simulations[30,31] of vesicles interacting with several particles of identical size and adhesive strength. In ref. 32, the stability of such tubes was studied systematically for the case of a membrane without spontaneous curvature, and was found to be strongly dependent on the range of the adhesive potential between the particles and the membrane. As the range of the adhesive potential was decreased, tubes were found to be more and more necklace-like, with narrower and narrower membrane

necks connecting adjacent engulfed particles, see Fig. 1(c). The stability limit of such necklace-like in-tubes was found numerically to approach $|W| = 2\kappa/R_{pa}^2$, as predicted by eqn (40) with $m = 0$.

4 Closed necks and adhesive substrates

4.1 Budding and tubulation of supported bilayers

So far, we have focused on the case of a large vesicle engulfing a small particle. The analytical treatment in Section 2.4 and, in particular, the stability condition (33) for a closed neck are however equally valid in the case in which the particle is larger than the vesicle. One example, for which the neck stability becomes important, is the budding or tubulation of supported lipid bilayers, see Fig. 1(d). In this case, the planar substrate corresponds to the limit in which the particle size R_{pa} becomes infinite. The stability condition of the closed neck (33) then has the form

$$\sqrt{\frac{|W|}{2\kappa}} - \frac{1}{R_i} + 2m \geq 0 \qquad (41)$$

where $R_i = R_{bu}$ or R_{cy} represents the radius of the spherical bud or the cylindrical tube respectively. The signs of the second and third term on the left hand side of (41) correspond to exocytic engulfment because the planar substrate corresponds to the limit of a large particle located within a somewhat larger vesicle.

Such budding and tubulation processes have been observed[33–36] after asymmetric exposure of the supported membrane to ions or peptides that generate spontaneous curvature. Considering the energetic competition between bud or tube formation and adhesion, it was found in ref. 37 that the membrane will unbind from the adhesive substrate forming buds of radius $R_{bu} = 1/m$ or cylindrical tubes of radius $R_{cy} = 1/2m$ if the spontaneous tension $2\kappa m^2$ exceeds the adhesive strength $|W|$. To extend this analysis, we now ask whether such budded or tubulated configurations are metastable for lower values of the spontaneous curvature, and could be obtained, *e.g.*, *via* mechanical pulling.

In the case of spherical buds, the radius R_{bu} of the bud must satisfy the normal force balance equation $\Delta P = 2(\Sigma + 2\kappa m^2)/R_{bu} - 4\kappa m/R_{bu}^2$, whereas in the case of a cylindrical tube, the cylinder radius R_{cy} must satisfy its corresponding normal balance equation $\Delta P = (\Sigma + 2\kappa m^2)/R_{cy} - \kappa/2R_{cy}^3$.[37,38]‡ In both cases, ΔP is the difference between the osmotic pressures in the interior and exterior solutions and Σ the membrane tension.

For a supported lipid bilayer, tangential force balance implies the mechanical tension $\Sigma = |W| - 2\kappa m^2$. Furthermore, if we include a water layer of finite thickness ℓ_w between the membrane and the substrate, the volume $V \approx \ell_w A$ for large A. Because the water layer thickness is determined by the molecular interactions between the membrane and the substrate, the volume V can no longer be varied independently of the area A and it becomes meaningless to include the Lagrange multiplier ΔP conjugate to the volume.

Using $\Delta P = 0$ and $\Sigma + 2\kappa m^2 = |W|$ in the two normal force balance equations for a spherical bud and a cylindrical tube, we find $R_{bu} = 2\kappa m/|W|$ for the radius of the bud and $R_{cy} = \sqrt{\kappa/2|W|}$ for the radius of the cylinder. Now, substituting the radius R_i in eqn (41) by these equilibrium values of R_{bu} and R_{cy}, we find the same stability relation

$$2\kappa m^2 \geq |W|/4 \qquad (42)$$

for the closed neck connecting spherical buds and cylindrical tubes to the supported bilayer.

In the case of cylindrical tubes, however, one also needs to consider the tangential force balance of the tube, that is, whether a tube will tend to grow indefinitely, whether there will be an equilibrium tube length, or whether the tube will shrink into a spherical bud. With $\Delta P = 0$ and $\Sigma + 2\kappa m^2 = |W|$, and using the equilibrium value of the cylinder radius R_{cy}, tangential balance shows that cylindrical tubes will grow indefinitely (in practice, until all the supported bilayer has been transferred into the tube) if $2\kappa m^2 > |W|$, but will shrink into a spherical bud with radius $R_{bu} = 2\kappa m/|W|$ otherwise. This instability towards spherical buds is intrinsic to cylindrical tubes, and is independent of the stability of the closed neck connecting the tube to the supported bilayer.

In summary, we predict that budded states are unstable for $2\kappa m^2 < |W|/4$, metastable in the interval $|W|/4 \leq 2\kappa m^2 \leq |W|$, and stable when $2\kappa m^2 > |W|$. Cylindrical tubes, on the other hand, are unstable for $2\kappa m^2 \leq |W|$, but can grow if $2\kappa m^2 > |W|$. It is also important to stress that, whereas the condition (42) and consequently these stability ranges depend on the particular choice of $\Delta P = 0$ and $\Sigma + 2\kappa m^2 = |W|$, the stability condition (41) is independent of this choice. Therefore, even if in a given experimental system it were unclear whether these assumptions are correct, the condition (41) would remain valid and could be used to obtain lower bounds on the substrate adhesive strength or the membrane spontaneous curvature by simply measuring the bud or cylinder radius.

4.2 Budding of supported bilayers from patterned substrates

At first sight, eqn (41) and (42) seem to be incompatible. According to (41), and to the results on particle engulfment in Section 3, the adhesiveness of the substrate should contribute to the stability of closed necks; however, according to (42), substrate adhesiveness ultimately acts to destabilize closed necks. This puzzling contradiction is solved by noticing that, in the case of budding of a supported bilayer, adhesion acts in two opposing ways: locally, it acts to stabilize closed necks as dictated by (41); globally, it sets the membrane tension and thus the bud size $R_{bu} = 2\kappa m/|W|$. This decrease in bud size with increasing substrate adhesion leads to an indirect destabilization of closed necks *via* (41).

‡ The normal force balance equations for spheres and cylinders can be obtained in a simple manner by minimizing the bending energies of these shapes with respect to their radii.[37] Alternatively, the same equations are obtained by specifying the Euler–Lagrange equation of the spontaneous curvature model[38] to these shapes.

These two effects can be disentangled by considering the budding of supported bilayers from patterned substrates, see Fig. 6. In this case, the substrate with 'global' adhesiveness $|W|$ contains a chemically distinct surface domain that displays a different, 'local' adhesiveness $|W_{\rm loc}|$. The stability condition for the closed neck connecting a spherical bud of radius $R_{\rm bu}$ to the supported bilayer within the surface domain is

$$\sqrt{\frac{|W_{\rm loc}|}{2\kappa}} - \frac{1}{R_{\rm bu}} + 2m \geq 0. \qquad (43)$$

On the other hand, the membrane tension is still defined by the global substrate adhesiveness, with $\Sigma = |W| - 2\kappa m^2$, and the equilibrium bud radius will therefore be $R_{\rm bu} = 2\kappa m/|W|$, as in the case of a homogeneous substrate. As a consequence, a larger local adhesiveness $|W_{\rm loc}|$ unequivocally increases the stability of buds within the surface domain.

By substituting the equilibrium value of $R_{\rm bu}$ into (43), we can rewrite the neck stability condition as

$$2\kappa m^2 \geq \left(\sqrt{|W_{\rm loc}| + 8|W|} - \sqrt{|W_{\rm loc}|}\right)^2 \Big/ 16 \qquad (44)$$

which directly shows that the stability of spherical buds is enhanced by an increase in local adhesiveness $|W_{\rm loc}|$. By setting $|W_{\rm loc}| = |W|$, we recover the condition (42) for homogeneous substrates. If $|W_{\rm loc}| > |W|$, the threshold of spontaneous tension $2\kappa m^2$ at which buds become metastable is lowered, and can be made arbitrarily low as the local adhesiveness is increased. Indeed, for very large local adhesiveness $|W_{\rm loc}| \gg |W|$ the stability condition (44) behaves as $2\kappa m^2 \gtrsim |W|^2/|W_{\rm loc}|$. Conversely, if the local adhesiveness is weaker than the global one, $|W_{\rm loc}| < |W|$, the spontaneous tension threshold is raised. In the limit of a non-adhesive surface domain with $|W_{\rm loc}| = 0$, the stability condition (44) becomes $2\kappa m^2 \geq |W|/2$.

Adhesive surface domains can thus be used to enhance the stability of spherical buds in supported bilayers. The threshold at which spherical buds become energetically favorable is still given by the global substrate adhesiveness, with $2\kappa m^2 > |W|$ as in ref. 37. Likewise, the stability of cylindrical tubes is still dictated by the global substrate adhesiveness, with tubes being unstable and shrinking for $2\kappa m^2 \leq |W|$, but growing for $2\kappa m^2 > |W|$.

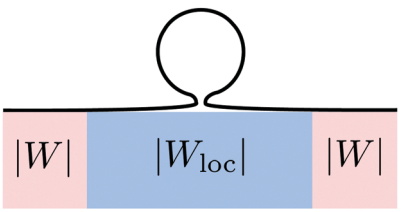

Fig. 6 Budding of a supported lipid bilayer from a patterned substrate. The substrate (pink region) with the 'global' adhesiveness $|W|$ contains a chemically distinct surface domain (blue region) that displays a different, 'local' adhesiveness $|W_{\rm loc}|$. The narrow neck that connects the spherical bud to the supported bilayer is located within the surface domain.

4.3 Giant plasma membrane vesicles

A similar budding geometry applies to the formation of giant plasma membrane vesicles (GPMVs) from cells *via* chemically induced blebbing. GPMVs are micrometer-sized spherical vesicles formed from the plasma membrane of eukaryotic cells that appear on the cell surface after treatment with a blebbing solution containing formaldehyde, dithiothreitol and Ca^{2+}.[19–22] In ref. 22, the mechanism of GPMV formation was studied in some detail. It was concluded that this blebbing solution causes a loss of membrane asymmetry and of actin cortex remodelling capabilities. As a consequence, the osmotic pressure can no longer be balanced by the cell cortex and blebs are formed. Before being cleaved off, the membrane will again form a narrow neck that must close in the presence of the adhesive cell cortex, see Fig. 1(e).

If the membrane asymmetry is lost as for the blebbing solution applied in ref. 22, the spontaneous curvature m vanishes. Using $m = 0$ in the exocytic version of the stability condition (33) and replacing $1/R_{\rm pa}$ by the mean curvature $M_{\rm cell}$ of the cell at the position of the neck as well as M' by the inverse radius $1/R_{\rm GPMV}$ of the spherical bleb, the stability condition for the closed neck of the bleb becomes

$$\sqrt{\frac{|W|}{2\kappa}} - M_{\rm cell} - \frac{1}{R_{\rm GPMV}} \geq 0. \qquad (45)$$

The bleb radius $R_{\rm GPMV}$ is controlled, in general, by a non-zero osmotic pressure difference between the inside and the outside of the cell, as well as by the cell membrane tension, both of which can be independently regulated by the cell and are not directly connected to the membrane-cortex adhesion $|W|$.[43] For this reason, it is expected that membrane-cortex adhesion will always act to stabilize the closed neck connecting the GPMV to the cell membrane. If the adhesion between the membrane and the cortex is too low, such that $\sqrt{|W|/2\kappa} < M_{\rm cell}$, the stability condition (45) cannot be satisfied and GPMV formation is not possible. On the other hand, for given values of $|W|$ and $M_{\rm cell}$, this stability condition is equivalent to $R_{\rm GPMV} \geq \left(\sqrt{|W|/2\kappa} - M_{\rm cell}\right)^{-1}$ and, thus, provides a lower threshold value for the observable radii $R_{\rm GPMV}$ of fully-formed, spherical GPMVs.

4.4 Outer membrane vesicles secreted by bacteria

The stability condition for closed necks can also be applied to the secretion of outer membrane vesicles (OMVs) by Gram-negative bacteria. These bacteria have a cell wall that consists of a peptidoglycan layer sandwiched between two lipid bilayers. During the secretion process, a large segment of the outer bilayer detaches from the peptidoglycan layer, bulges out towards the external medium, and forms a spherical vesicle that is released from the prokaryotic cell.[23] These vesicles have a variable radius between 25 and 125 nm, and their membranes are strongly asymmetric.[23] As a consequence, the membrane spontaneous curvature m cannot be neglected and the stability condition (33) for a spherical, fully-formed OMV of radius $R_{\rm OMV}$ becomes

$$\sqrt{\frac{|W|}{2\kappa}} - M_{\rm bact} - \frac{1}{R_{\rm OMV}} + 2m \geq 0. \qquad (46)$$

where $|W|$ is the adhesive strength of the interaction between the peptidoglycan layer and the outer bilayer, and M_{bact} is the mean curvature of the outer bilayer membrane at the position of the closed neck. Eqn (46) shows that, for given values of M_{bact} and R_{OMV}, the closed neck is stabilized by both the adhesive strength $|W|$ and a positive spontaneous curvature $m > 0$. The spontaneous curvature has already been proposed to be a driving force for OMV formation.[23,24] Our study shows that the adhesion of the membrane to the underlying peptidoglycan layer makes another important contribution to neck stability.

5 Neck stabilization by constriction forces

5.1 Externally applied constriction forces

In biological cells, many processes that involve the formation of membrane necks, such as particle endocytosis or exocytosis, involve proteins that generate constriction forces onto the necks,[11] see Fig. 7. In the case of endocytosis, proteins such as dynamin[16] or the ESCRT machinery[15] are typically associated with such forces. In phagocytosis, a 'purse string' composed of actin and myosin motors is usually present around the neck.[12]

Externally applied constriction forces around a membrane neck can be easily included in the analytical treatment of Section 2.4, by simply adding the axi-symmetric term $E_f = fR_{\mathrm{ne}}$ to the total energy of the system as given by (27). Here, a positive value of f corresponds to a constriction force perpendicular to the neck while a putative negative value of f acts to widen the neck.

Including the additional energy term $E_f = fR_{\mathrm{ne}}$ in the computation of Section 2.4, we obtain the generalized stability condition

$$\frac{f}{4\pi\kappa} + \sqrt{\frac{|W|}{2\kappa}} - \frac{1}{R_{\mathrm{pa}}} \pm M' \mp 2m \geq 0 \qquad (47)$$

for a closed membrane neck. The upper and lower signs of the $\pm$ and $\mp$ symbols again apply to endocytic and exocytic engulfment, respectively, see Fig. 1(a and b).

The generalized condition (47) implies that constriction forces with $f > 0$ promote the formation of closed necks.

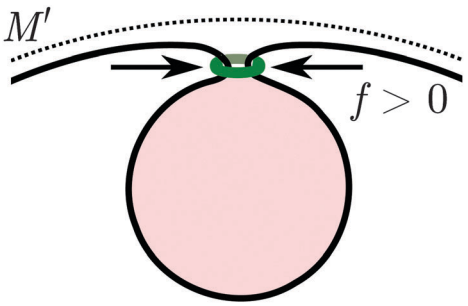

Fig. 7 Contractile ring (green), representing endocytosis-associated machinery, exerting a constriction force $f > 0$ perpendicular to the narrow membrane neck during particle engulfment. The mother membrane has mean curvature M' at the position of the neck.

In particular, constriction forces generated, *e.g.*, by active processes can be sufficient to close a neck even in the absence of any adhesive surface. Indeed, for $|W| = 0$, the condition (47) can be rewritten in the form

$$\frac{f}{4\pi\kappa} \geq \frac{f_{\mathrm{min}}}{4\pi\kappa} \equiv \frac{1}{R_{\mathrm{pa}}} \mp M' \pm 2m \qquad (48)$$

which defines the minimal constriction force f_{min} necessary for neck closure. Such minimal constriction forces were numerically studied in ref. 44, and we find that their numerical results are in complete agreement with the expression (48) for f_{min}.

It is also possible that constriction forces play a role in the budding of 'empty' vesicles in the presence of adhesive substrates, such as the actin cortex or the peptidoclycan layer as described in Sections 4.3 and 4.4. The corresponding stability conditions are obtained by adding the term $f/4\pi\kappa$ to the left hand side of (45) and (46).

5.2 Intrinsic engulfment force

Additional insight into closed membrane necks can be obtained by rewriting eqn (47) in the alternative form $f + f_{\mathrm{eng}} \geq 0$ with the intrinsic engulfment force f_{eng} for neck closure defined by

$$f_{\mathrm{eng}} \equiv 4\pi\kappa\left(\sqrt{\frac{|W|}{2\kappa}} - \frac{1}{R_{\mathrm{pa}}} \pm M' \mp 2m\right). \qquad (49)$$

As before, the upper and lower signs of the $\pm$ or $\mp$ symbols correspond to endocytic and exocytic engulfment, respectively.

The stability condition (33) now has the simple form $f_{\mathrm{eng}} \geq 0$ corresponding to the neck closure condition $f_{\mathrm{eng}} = 0$ and the closed neck condition $f_{\mathrm{eng}} > 0$. Thus, even for $f = 0$, *i.e.*, in the absence of externally applied constriction forces, the neck experiences the intrinsic engulfment force f_{eng} arising from the interplay of membrane-particle adhesion and curvature elasticity. This intrinsic force grows both with the adhesive strength and the particle size. It seems plausible to expect that such engulfment forces lower the barrier for the fission of the neck. Therefore, a larger value of f_{eng} should increase the probability for thermally-excited neck fission and vesicle cleavage.

6 Summary and conclusions

In this paper, we have shown that the presence of an adhesive surface strongly affects the stability of closed membrane necks. In the absence of an adhesive surface, previous research showed that closed necks could only be stable in membranes with bilayer asymmetry and/or intramembrane domains.[2,4,7,39] Our analytical and numerical results reveal that membrane adhesion in itself is already sufficient to stabilize closed necks. Furthermore, we have derived precise stability conditions for several systems of experimental relevance: (i) endocytic and exocytic engulfment of particles by membranes, see eqn (33); (ii) necklace-like particle-filled membrane tubes, see eqn (37) and (38); (iii) budding and tubulation of supported lipid bilayers from homogenous substrates, see eqn (41) and (42), as well as

from patterned substrates, see eqn (43) and (44); (iv) formation of giant plasma membrane vesicles *via* chemically induced blebbing, see eqn (45); (v) formation of outer membrane vesicles in Gram-negative bacteria, see eqn (46); and (vi) particle engulfment with externally applied constriction forces, see eqn (47). Finally, we showed that constriction forces can be sufficient to stabilize closed necks even in the absence of adhesion, see eqn (48), and introduced an intrinsic engulfment force that directly describes the effect of curvature elasticity and membrane-substrate adhesion on neck closure, see eqn (49). Whenever possible, we have validated the predictions of our analytical stability conditions against numerical results found in the literature.

Throughout the paper, we discussed the stability conditions for closed necks in the context of the spontaneous curvature model, which assumes that the area difference between the two leaflets of the membrane can change *via* lipid flip-flops. This assumption is valid for multi-component membranes containing sterols such as cholesterol because the latter molecules undergo fast flip-flops between the leaflets on the timescale of a second. For membranes containing only phospholipids, on the other hand, flip-flops occur much more slowly, and the area difference between the two leaflets has a certain preferred value on the typical timescales of experiments, a constraint that is incorporated in the area-difference-elasticity model.[45] As discussed in ref. 46, the stability conditions for closed necks described here are also valid in the area-difference-elasticity model provided we replace the spontaneous curvature m by the effective spontaneous curvature $m_{\mathrm{eff}} \equiv m + \pi(\kappa_\Delta/\kappa)(I_0 - I)/A$, where A is the membrane area, κ_Δ is a second bending rigidity,[45] and $I \equiv \int \mathrm{d}A M$ is the integrated mean curvature, which attains the value I_0 when the area difference between the two leaflets is optimal. The parameter κ_Δ is a material parameter, the parameter I_0 is determined by the preparation procedure and is, thus, difficult to control, while the integrated mean curvature I depends on the membrane shape, and thus on the size of the particles or membrane buds under consideration. These modified stability conditions can also be obtained directly from the analytical model in Section 2.4 by explicitly including the energetic contribution of the area difference elasticity in the total energy (27). In any case, we find that adhesive surfaces and constriction forces act to stabilize closed necks independently of the curvature model.

It seems appealing to generalize the stability condition (33), as well as the stability conditions described in Section 3.3, to the engulfment of non-spherical particles by simply substituting the inverse particle radius $1/R_{\mathrm{pa}}$ by the local mean curvature M_{pa} that varies along the particle surface. This particle mean curvature is positive everywhere for convex particles, such as prolate or oblate ellipsoids; however, it can also be negative if the particle surface includes concave surface segments, *e.g.*, around the poles of a discocyte-shaped particle. As a consequence of the variation of the particle mean curvature along the particle surface, the neck stability condition will change along the particle surface, which implies that the neck stability depends on the position of the neck. Therefore, the surface of a particle may exhibit two or more surface domains corresponding to stable and unstable necks. The latter conclusion can be scrutinized by numerical methods. As a first example, consider the engulfment of ellipsoidal particles by planar membranes with zero spontaneous curvature as studied in ref. 47, with prolate and oblate ellipsoids constrained to have their symmetry axis parallel and perpendicular to the membrane, respectively. In this numerical study, completely engulfed states with closed necks were found to be (meta)stable whenever $|W| \geq 2\kappa M_{\mathrm{pa}}{}^2$, where M_{pa} was the mean curvature of the prolate and oblate ellipsoids at their equator and poles, respectively. These results are in complete agreement with the stability condition (33) when we put $M' = m = 0$ and replace the inverse particle radius $1/R_{\mathrm{pa}}$ by the local mean curvature M_{pa} of the particle surface.

The stability of closed necks as discussed here refers to their energetic stability against neck opening. A different question, which we hardly addressed here, is whether the closed neck will be stable against fission (or scission). Predicting whether the closed neck will break, leading to fission, or whether it will remain intact, leaving the topology of the membrane unchanged, lies beyond the realm of applicability for the continuum membrane model used here. As an example, our continuum model allows for the formation of infinitely narrow membrane necks, whereas the diameter of a real neck must exceed twice the membrane thickness $\ell_{\mathrm{me}} \simeq$ 4–5 nm. In practice, the continuum model becomes inaccurate for neck sizes of the order of a few times the membrane thickness ℓ_{me}, and corrections to the model will stabilize the neck size at a finite non-zero value, somewhat larger than ℓ_{me}. Understanding the fission step in detail requires modelling at the molecular level.[48–50] In any case, our results provide a necessary condition for membrane fission, and will remain valid as long as the particles or membrane buds are large compared to the membrane thickness. It will also be interesting to see whether the intrinsic engulfment force as given by (49) can be related to the energy barrier for neck fission.

In experiments, the stability conditions described here can be used to estimate the adhesive strength of the membrane-surface interaction or the membrane spontaneous curvature, whenever fission or a closed neck are observed. Indeed, in most experiments the radii of the particles or curvature of the membranes involved can be measured optically. If the spontaneous curvature of the membrane is known, observation of a closed neck directly implies a minimal value of the adhesive strength *via* the stability conditions presented here. Conversely, if the adhesive strength is known, the stability conditions can be used to obtain a lower or upper estimate for the membrane spontaneous curvature. Furthermore, it will often be possible to directly observe the process of neck closure, and we can then use the equalities in the stability relations (33), (37), (38), (41), (43), (45) and (46) to obtain improved estimates for the different material parameters.

The stability condition for closed membrane necks in particle engulfment as given by eqn (33) has already proven useful in order to understand the size-dependence of endocytosis[17] and the interaction of nanoparticles with membranes of complex shape.[46] As shown here, analogous stability conditions are relevant for many different processes. As a consequence, adhesion

should play an essential role in the formation and closure of narrow necks by biomimetic and biological membranes.

Acknowledgements

This study was supported by the German Research Foundation (DFG) *via* the IRTG 1524 and by the Federal Ministry of Education and Research (BMBF) *via* the consortium MaxSynBio.

References

1 K. Berndl, J. Käs, R. Lipowsky, E. Sackmann and U. Seifert, *Europhys. Lett.*, 1990, **13**, 659–664.
2 U. Seifert, K. Berndl and R. Lipowsky, *Phys. Rev. A: At., Mol., Opt. Phys.*, 1991, **44**, 1182–1202.
3 L. Miao, B. Fourcade, M. Rao, M. Wortis and R. K. P. Zia, *Phys. Rev. A: At., Mol., Opt. Phys.*, 1991, **43**, 6843–6856.
4 B. Fourcade, L. Miao, M. Rao, M. Wortis and R. K. P. Zia, *Phys. Rev. E: Stat. Phys., Plasmas, Fluids, Relat. Interdiscip. Top.*, 1994, **49**, 5276–5286.
5 Y. Liu, J. Agudo-Canalejo, A. Grafmüller, R. Dimova and R. Lipowsky, *ACS Nano*, 2016, **10**, 463–474.
6 R. Lipowsky, *J. Phys. II*, 1992, **2**, 1825–1840.
7 F. Jülicher and R. Lipowsky, *Phys. Rev. Lett.*, 1993, **70**, 2964–2967.
8 T. Baumgart, S. T. Hess and W. W. Webb, *Nature*, 2003, **425**, 821–824.
9 R. Bar-Ziv and E. Moses, *Phys. Rev. Lett.*, 1994, **73**, 1392–1395.
10 H. T. McMahon and J. L. Gallop, *Nature*, 2005, **438**, 590–596.
11 J. H. Hurley, E. Boura, L.-A. Carlson and B. Różycki, *Cell*, 2010, **143**, 875–887.
12 J. A. Swanson, M. T. Johnson, K. Beningo, P. Post, M. Mooseker and N. Araki, *J. Cell Sci.*, 1999, **112**, 307–316.
13 I. Mendes Pinto, B. Rubinstein, A. Kucharavy, J. R. Unruh and R. Li, *Dev. Cell*, 2012, **22**, 1247–1260.
14 R. Knorr, R. Lipowsky and R. Dimova, *Autophagy*, 2015, **11**, 2134–2137.
15 J. H. Hurley and P. I. Hanson, *Nat. Rev. Mol. Cell Biol.*, 2010, **11**, 556–566.
16 S. M. Ferguson and P. De Camilli, *Nat. Rev. Mol. Cell Biol.*, 2012, **13**, 75–88.
17 J. Agudo-Canalejo and R. Lipowsky, *ACS Nano*, 2015, **9**, 3704–3720.
18 H. Kalra, G. P. C. Drummen and S. Mathivanan, *Int. J. Mol. Sci.*, 2016, **17**, 170.
19 R. E. Scott, *Science*, 1976, **194**, 743–745.
20 T. Baumgart, A. T. Hammond, P. Sengupta, S. T. Hess, D. A. Holowka, B. A. Baird and W. W. Webb, *Proc. Natl. Acad. Sci. U. S. A.*, 2007, **104**, 3165–3170.
21 S. L. Veatch, P. Cicuta, P. Sengupta, A. Honerkamp-Smith, D. Holowka and B. Baird, *ACS Chem. Biol.*, 2008, **3**, 287–293.
22 H. Keller, M. Lorizate and P. Schwille, *ChemPhysChem*, 2009, **10**, 2805–2812.
23 A. Kulp and M. J. Kuehn, *Annu. Rev. Microbiol.*, 2010, **64**, 163–184.
24 J. W. Schertzer and M. Whiteley, *mBio*, 2012, **3**, e00297.
25 C. Dietrich, M. Angelova and B. Pouligny, *J. Phys. II*, 1997, **7**, 1651–1682.
26 K. Jaskiewicz, A. Larsen, D. Schaeffel, K. Koynov, I. Lieberwirth, G. Fytas, K. Landfester and A. Kroeger, *ACS Nano*, 2012, **6**, 7254–7262.
27 A. Meinel, B. Tränkle, W. Römer and A. Rohrbach, *Soft Matter*, 2014, **10**, 3667–3678.
28 R. Michel, E. Kesselman, T. Plostica, D. Danino and M. Gradzielski, *Angew. Chem., Int. Ed.*, 2014, **53**, 12441–12445.
29 F. G. Strobl, F. Seitz, C. Westerhausen, A. Reller, A. A. Torrano, C. Bräuchle, A. Wixforth and M. F. Schneider, *Beilstein J. Nanotechnol.*, 2014, **5**, 2468–2478.
30 A. H. Bahrami, R. Lipowsky and T. R. Weikl, *Phys. Rev. Lett.*, 2012, **109**, 188102.
31 A. Šarić and A. Cacciuto, *Phys. Rev. Lett.*, 2012, **109**, 188101.
32 M. Raatz, R. Lipowsky and T. R. Weikl, *Soft Matter*, 2014, **10**, 3570–3577.
33 Y. A. Domanov and P. K. J. Kinnunen, *Biophys. J.*, 2006, **91**, 4427–4439.
34 L. R. Cambrea and J. S. Hovis, *Biophys. J.*, 2007, **92**, 3587–3594.
35 A. Arouri, V. Kiessling, L. Tamm, M. Dathe and A. Blume, *J. Phys. Chem. B*, 2010, **115**, 158–167.
36 T. J. Pucadyil and S. L. Schmid, *Biophys. J.*, 2010, **99**, 517–525.
37 R. Lipowsky, *Faraday Discuss.*, 2013, **161**, 305–331.
38 Z.-C. Ou-Yang and W. Helfrich, *Phys. Rev. A: At., Mol., Opt. Phys.*, 1989, **39**, 5280–5288.
39 F. Jülicher and R. Lipowsky, *Phys. Rev. E: Stat. Phys., Plasmas, Fluids, Relat. Interdiscip. Top.*, 1996, **53**, 2670–2683.
40 W. Helfrich, *Z. Naturforsch., C: J. Biosci.*, 1973, **28**, 693–703.
41 U. Seifert and R. Lipowsky, *Phys. Rev. A: At., Mol., Opt. Phys.*, 1990, **42**, 4768–4771.
42 M. Deserno, *Phys. Rev. A: At., Mol., Opt. Phys.*, 2004, **69**, 031903.
43 J. Dai and M. P. Sheetz, *Biophys. J.*, 1999, **77**, 3363–3370.
44 B. Božič, J. Guven, P. Vázquez-Montejo and S. Svetina, *Phys. Rev. A: At., Mol., Opt. Phys.*, 2014, **89**, 052701.
45 L. Miao, U. Seifert, M. Wortis and H.-G. Döbereiner, *Phys. Rev. E: Stat. Phys., Plasmas, Fluids, Relat. Interdiscip. Top.*, 1994, **49**, 5389–5407.
46 J. Agudo-Canalejo and R. Lipowsky, *Nano Lett.*, 2015, **15**, 7168–7173.
47 S. Dasgupta, T. Auth and G. Gompper, *Soft Matter*, 2013, **9**, 5473–5482.
48 J. Shillcock and R. Lipowsky, *Biophys. Rev. Lett.*, 2007, **2**, 33–55.
49 A. Grafmüller, J. C. Shillcock and R. Lipowsky, *Biophys. J.*, 2009, **96**, 2658–2675.
50 K. Yang and Y.-Q. Ma, *Soft Matter*, 2012, **8**, 606–618.

